Positional accuracy as a measure of *Chandra*'s optical distortions

E. Beckerman, T. Aldcroft, T. J. Gaetz, D. Jerius, D. Nguyen, M. Tibbetts

Harvard-Smithsonian Center for Astrophysics, Cambridge, MA 02138, USA

ABSTRACT

We present a study of *Chandra*'s optical distortions by examining the positional accuracy of observed sources on the HRC-I. We investigate the *Chandra* mirror and detector models' ability to reproduce the detector locations of observed sources by simulating ∼160 calibration observations of AR Lac, HR 1099, and LMC X-1. To study the optical distortions of the mirrors more directly, we compare a 63 ksec observation of the Orion Nebular Cluster (ONC) with positions based on the well-determined optical astrometry of the cluster. We simulate observations of 100 reasonably bright sources from the Hillenbrand 1997[1] catalog of the ONC and compare the simulated positions with their observed positions. Offsets between the optical positions and the observed X-ray positions help determine a map of the optical distortions of the *Chandra* mirrors.

Keywords: *Chandra*, HRMA, Optical Distortions, Positional Accuracy, X-ray Optics

1. INTRODUCTION

In an effort to understand how the *Chandra* X-ray Observatory images a grid of sources to the detector plane, we examine the positional accuracy of observed sources on the HRC-I. The HRC-I, a microchannel plate detector, has a single imaging element which is flat, and tangent to the on-axis focal surface of the system. The other *Chandra* detectors are composed of multiple, tilted, elements; the HRC-I avoids these geometrical complexities and provides the simplest interpretations of deviations from the ideal optics. To further simplify the analysis, we use the CHIP coordinates of the HRC-I, which are based directly on the detector hardware, and are independent of tangent plane corrections, or any assumptions of platescale or optical distortions. CHIP coordinates have the most natural correspondence to the telescope coordinates and optical source positions. Unfortunately, they are not entirely independent of *Chandra* calibration, as CHIP positions are determined using the HRC degap map.

Chandra has subarcsecond absolute astrometry for sources with off-axis angles less than 3 arcminutes.[5] Further off-axis, complications such as the broad point spread function (PSF), deviations of the detector from the focal surface, and other asymmetries diminish the astrometric accuracy. Producing a map of the optical distortions of *Chandra*'s High Resolution Mirror Assembly (HRMA) is therefore a complex project and it is necessary to isolate contributions from the mirrors, detectors, and the *Chandra* X-ray Center's (CXC) models for both.

We present two independent studies of *Chandra*'s positional accuracy and the precision to which the CXC telescope and detector models can reproduce the observed detector positions of point sources on the HRC-I. The first study examines calibration observations of the bright point sources AR Lac, HR 1099, and LMC X-1, while the second examines a star field with known relative positions – the Orion Nebular Cluster. Both studies test the ability of the CXC mirror and detector models to predict where the telescope would image the sources to the detector plane, but the ONC observation provides a more direct examination of the optical distortions of the mirrors.

Send correspondence to E.B.
E-mail: ebeckerman@cfa.harvard.edu, Telephone: 617 495 7366

2. OBSERVATIONS AND CENTROIDS

2.1. Individual Bright Point Sources

We incorporate all archived HRC-I observations of the bright point sources AR Lac, HR 1099, and LMC X-1 which have no translation of the Science Instrument Module (SIM). There were 139, 17, and 6 available observations, respectively, for these sources.

Since the CHIP coordinates are in the reference frame of the detector, the telescope's dither pattern must be removed manually. Breaking each observation into 100-second bins, we fit the time-varying position of the object's center and subtract this fit from the data to get corrected CHIP positions for all events. Once the telescope motion is removed from the detector coordinates, we use a sigma-clipping algorithm to determine an accurate centroid for the source. Because the CHIP coordinate system is based on the hardware of the HRC, these centroids provide an accurate measure of where the observations fell on the detector.

We then use the CIAO[3] tool *dmcoords* to convert these positions into Mirror Spherical Coordinates (MSC),[4] or θ and ϕ – the off-axis and azimuthal angles of the source, respectively. These coordinates were then used to perform the raytraces described in §3.

2.2. Orion Nebular Cluster

While studying individual bright point source observations is helpful in comparing the on-orbit performance of the telescope to the CXC models, random aspect errors between observations may exist, and there is no straightforward way to account for these. A better approach is to use a cluster of stars with well-determined relative positions from optical astrometry. We use a 63 ksec observation of the Orion Nebular Cluster on the HRC-I (OBSID 26) from February 2000. This avoids aspect errors between observations, and better isolates the contribution from *Chandra*'s mirrors to positional inaccuracies.

In removing the dither pattern from the image in CHIP coordinates, we use SKY coordinates of the brightest source in the field – the central star θ^1 Ori C – as a filter. With a count rate of $\sim$1.9 counts per second, this source provides sufficient signal to provide a good time-averaged fit to subtract from the data. Figure 1 shows a comparison of the de-dithered image in CHIP coordinates with the SKY coordinates image created from the standard processing pipeline. Once the dither has been removed from the observation, we use the same sigma-clipping algorithm to determine source centroids, though with a smaller initial clipping radius to avoid source overlap in this crowded field.

For the optical positions of the stars in the ONC, we use the Hillenbrand 1997[1] catalog, which covers the entire $30'$ x $30'$ HRC-I field. While the astrometry of this catalog is internally consistent, Hillenbrand & Carpenter 2000[2] point out that the astrometry was derived from the HST Guide Star Catalog, and is offset by about $1.5''$ from their 2000 ONC catalog which is properly referenced to the ACT Reference Catalog. Unfortunately, while overlayed positions from the Hillenbrand & Carpenter 2000 catalog on the HRC observation match well, this catalog does not cover most of the field. We therefore perform a plate-solution fit to shift the Hillenbrand 1997 catalog to the 2000 catalog positions. We find very good agreement between these resultant optical positions and the observed *Chandra* sources. Figure 2 shows 3 off-axis X-ray sources with the positions from optical astrometry marked off.

We initially selected 114 reasonably bright X-ray sources with > 300 counts, which have clear-cut optical identifications.[6] Using the astrometric positions derived from the Hillenbrand 1997 catalog, we used *dmcoords* to predict the CHIP position of the source. We also use the astrometric positions and the nominal pointing of the *Chandra* observation to derive θ and ϕ for the raytraces. We find that there is an offset of $\sim 2.5''$ between the CHIP coordinates determined by *dmcoords* and those of the observed centroids. While the cause of the offset is not known, we have learned that the Aspect Camera Assembly's (ACA) fiducial lights have drifted by about $10''$ since launch.[7] This either means there has been a shift between the detectors and the telescope optics that *dmcoords* does not account for, or the aspect camera itself has tilted. This time-dependent drift could also impact the analysis for the individual bright point source observations.

For the purposes of this analysis we simply apply the $2.5''$ offset to the positions of the observed centroids of ONC sources. We further narrowed our sample of stars by excluding 14 sources whose corrected centroid

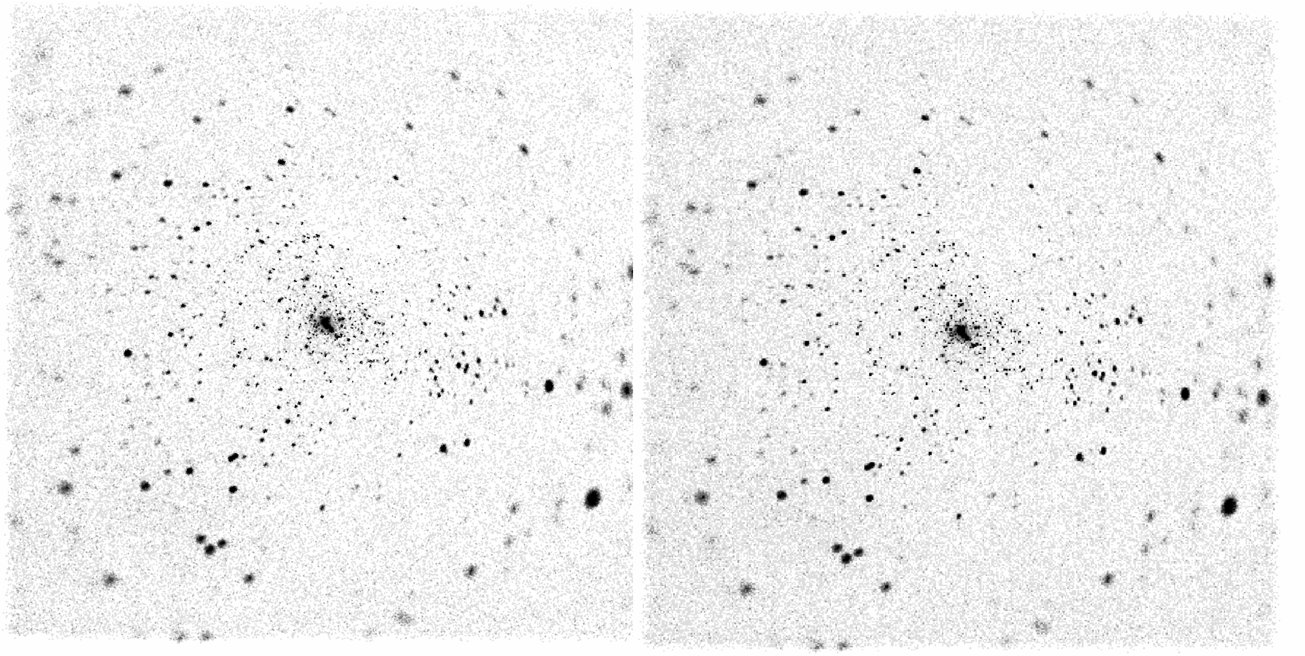

Figure 1. LEFT: The Orion Nebular Cluster on HRC-I, in SKY coordinates, as determined by standard pipeline processing. RIGHT: ONC on HRC-I in CHIP coordinates, after telescope dither is manually removed.

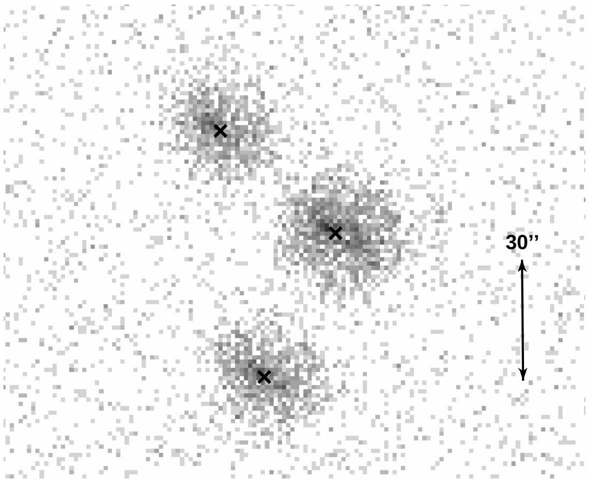

Figure 2. 3 sources in the ONC which are about 12 arcminutes off-axis, binned by 8 HRC pixels. The crosses mark the positions from the optical astrometry of the Hillenbrand 1997 catalog, shown to line up with the *Chandra* sources.

locations were $> 3''$ from the chip position predicted by *dmcoords*. These tended to have relatively poor signal-to-noise and broad PSFs. We thus use a final sample of 100 sources in the Orion Nebular Cluster, with well-determined optical astrometry, which can be compared to the centroided CHIP positions of the observations as well as simulations based on CXC mirror and detector models.

3. SIMULATIONS

On-orbit performance of the *Chandra* mirrors is best understood by utilizing the *SAOsac*[8] software suite to run simulations of observations. Developed by the CXC Optics Group to provide a high-fidelity model for the HRMA, *SAOsac* allows detailed interpretations of in-flight *Chandra* data. In addition to the *SAOsac* model of the HRMA, there is a *MARX*[9] mirror model which has been widely used to simulate *Chandra* performance and to aid in writing proposals. *MARX* was developed by the MIT/CXC group to provide a detailed raytrace simulation of the HETG performance, and is essentially a simplified version of the *SAOsac* model. *MARX* also includes models of the *Chandra* gratings and detectors. *SAOsac* raytraces a source based on the off-axis and azimuthal angles, while *MARX* takes as input the nominal pointing (RA, Dec, and telescope ROLL), and the source RA and Dec.

For the sake of comparison, our analysis incorporates 3 different detector models: *MARX* (MIT/CXC), *psf_project_ray*[10] (CIAO), and *deticpt*[11] (CXC Optics engineering model). *SAOsac* rays may be sent through all 3 of these detector models, while *MARX* rays are projected to the HRC-I only with the *MARX* detector model. Each raytrace typically has ∼10,000 detected counts, and we use the same centroiding technique on both the simulated data and the observations. We found the positions of the simulated sources to be sensitive to the random number seed used in both *MARX* and *SAOsac*, and so we ran 100 realizations of this experimental setup for both the individual point source observations and the Orion Nebular Cluster observation.

For the individual bright point sources, we use θ, ϕ, RA, and Dec determined by *dmcoords* based on the centroided CHIP coordinates for the source. For the ONC sources, we use the astrometric positions of the 100 sources, which are entirely independent of the *Chandra* observation. We can then compare the observed chip positions of each source with the raytraced detector locations. Furthermore, for the ONC observation, we can compare the simulated and observed positions with those determined by *dmcoords*, based upon the optical astrometry for those sources.

4. ANALYSIS AND RESULTS

4.1. Positional Offsets

Visual comparisons of the positional offsets between the observations and simulations are helpful in portraying the existence of any inconsistencies or optical distortions which are not accounted for by the telescope models. Figure 3 shows vector diagrams, for the individual sources from §2.1, of the positional shifts between the observed CHIP positions and those simulated using θ and ϕ derived by *dmcoords* from those positions. We show all 4 combinations of mirror and detector models, for one random number seed. The arrows represent the offset between the observed CHIP positions and the simulations based on those positions, scaled by a factor of 1000 to emphasize the deviations. The apparent linear scaling of the offsets with distance indicates that there is a platescale effect.

Figures 4 and 5 present vector diagrams for the Orion Nebular Cluster shifts. Figure 4 presents a comparison between the observed CHIP positions of the ONC stars and the centroids of simulations based on their astrometric positions; Fig. 5 shows the shifts between the *dmcoords*-determined positions and the same simulations. We also make a comparison between observed positions (corrected for the $2.5''$ offset described in §2.2) of the ONC sources and their α and δ from the Hillenbrand 1997 catalog by feeding those to *dmcoords* to get CHIP coordinates. Figure 6 shows vectors from the centroids of observed sources to the *dmcoords* positions.

4.2. Spatial Transformation Functions

For a quantitative analysis of the offsets, we use the IRAF[12] tool *geomap* to perform fits of spatial transformation functions to the shifts between observations and simulations. The field of individual bright point source observations is easily divided into two groupings – those sources in the inner 5000x5000 pixel ($11'$ x $11'$) region of the HRC-I, and those outside this region. A look at Fig. 3 helps clarify the distinction. We run the *geomap* fits on these two regions separately, and indeed, they have different transformation characteristics. For the ONC sources, there is no natural separation, but we use the same region of the chip for consistency.

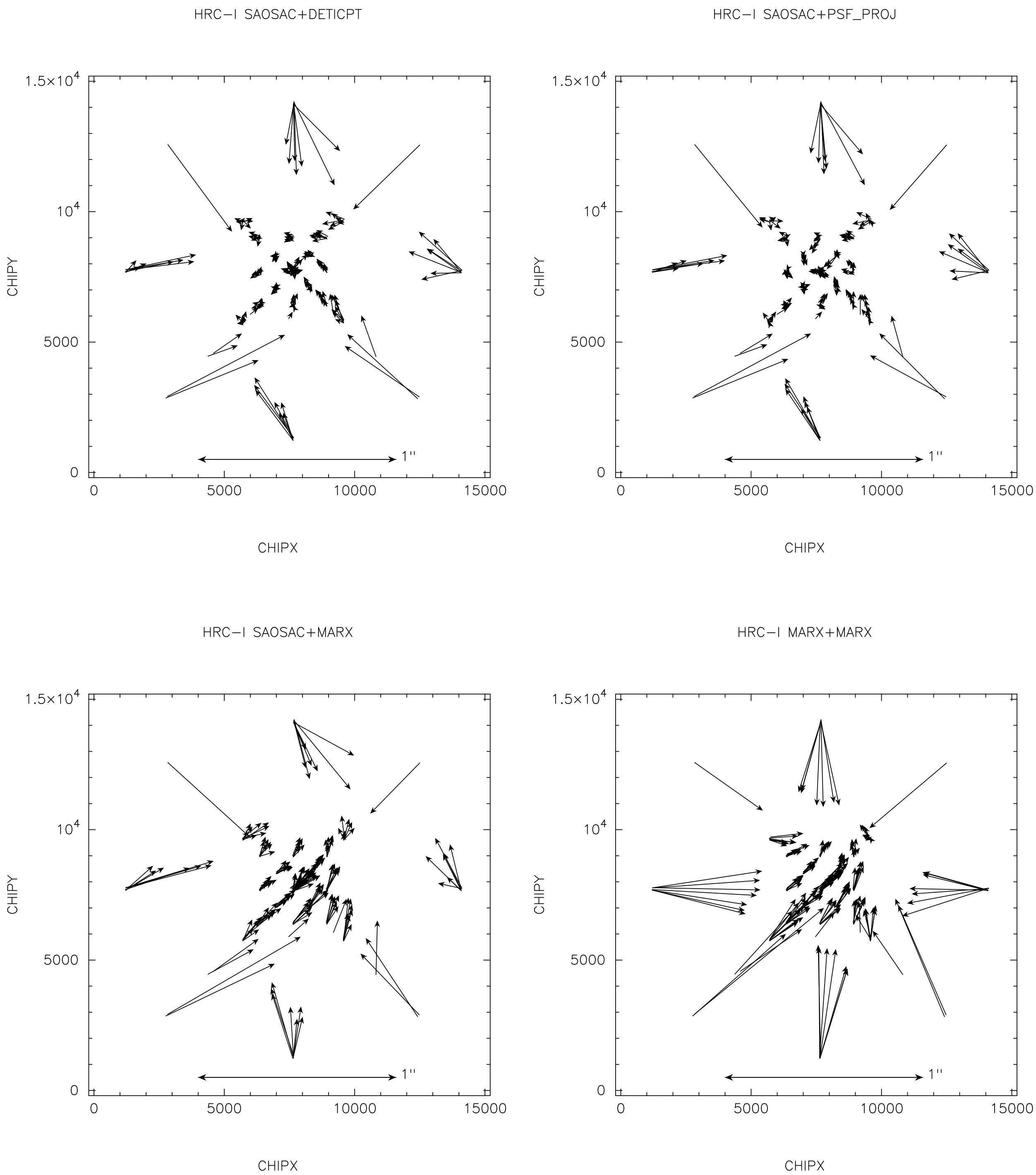

Figure 3. Individual bright point source observations: vector diagrams representing the shift from centroids of the observed detections to centroids of the simulated rays. Positional offsets are scaled by a factor of 1000 to exaggerate the deviations. The arrow at the bottom denotes shifts of $1''$ ($\sim$7.5 HRC pixels) in this scaling convention. Quantitative analysis of these offsets is shown in Table 1.

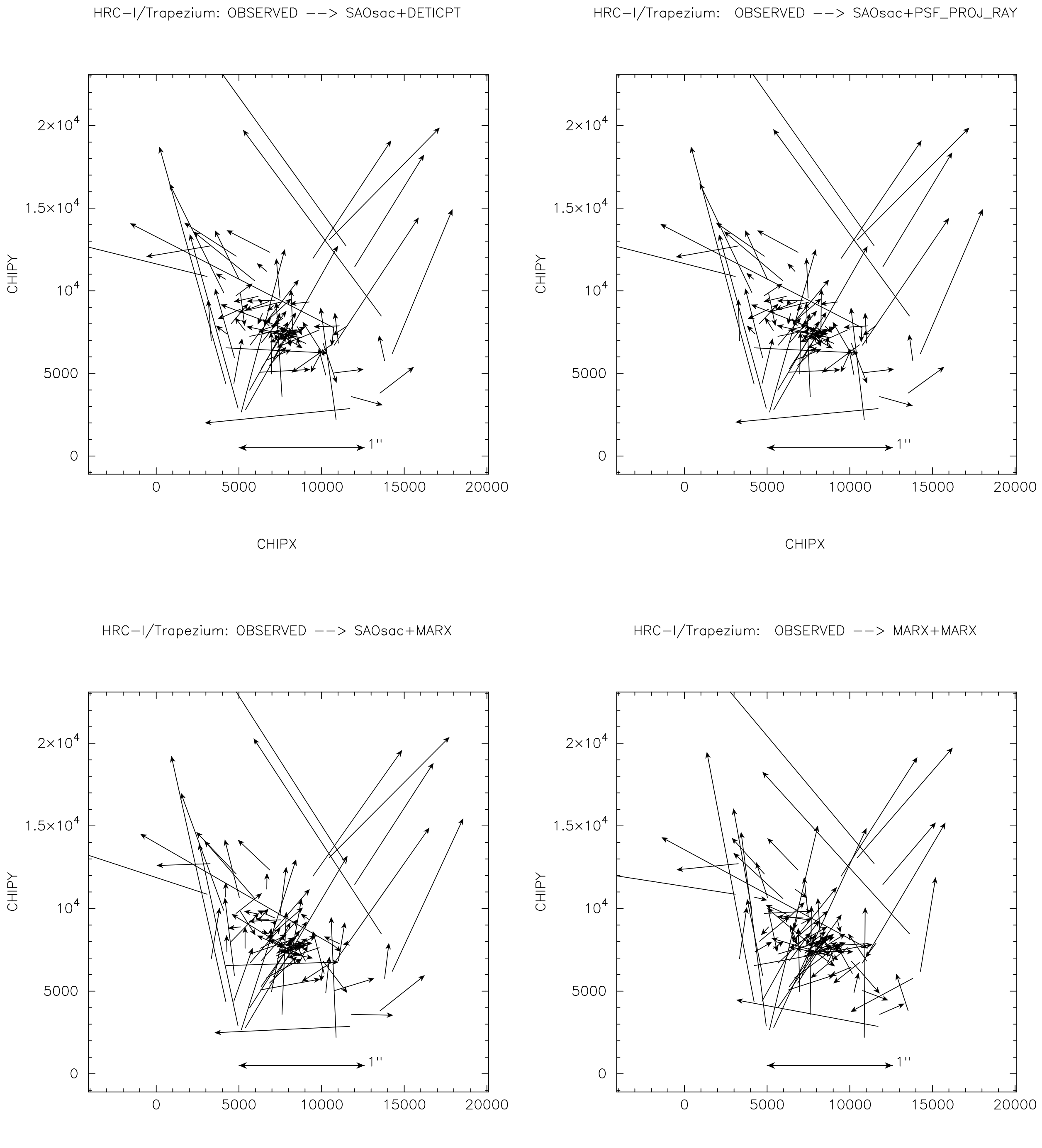

Figure 4. ONC: Positional shifts from where the sources were observed in CHIP coordinates to where the simulations placed them on the detector. The scaling convention follows that in Fig. 3.

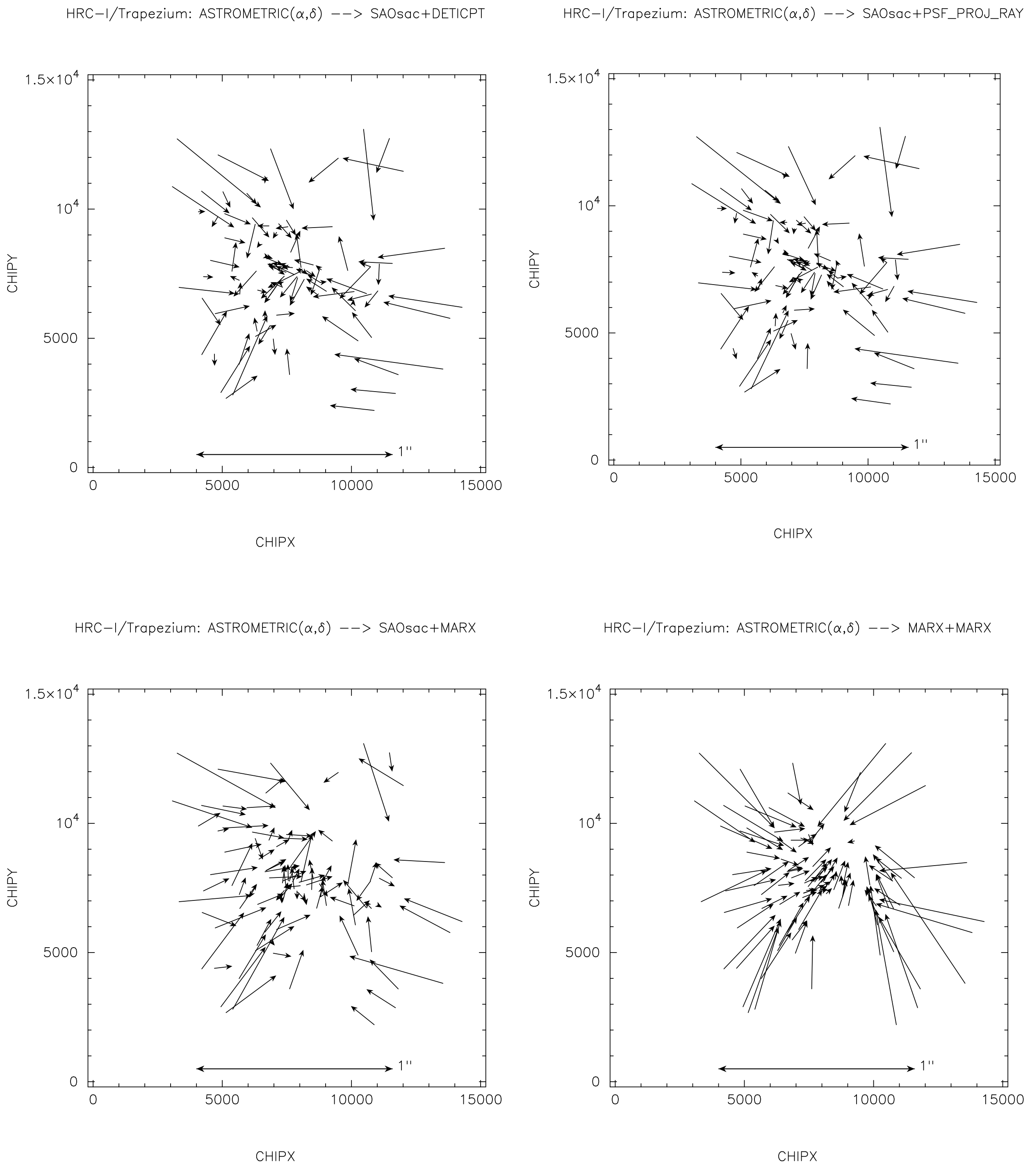

Figure 5. ONC: Positional shifts from CHIP positions determined by *dmcoords* based on the optical astrometry and the nominal pointing, to where the models predict they would be imaged. The scaling convention follows that in Fig. 3.

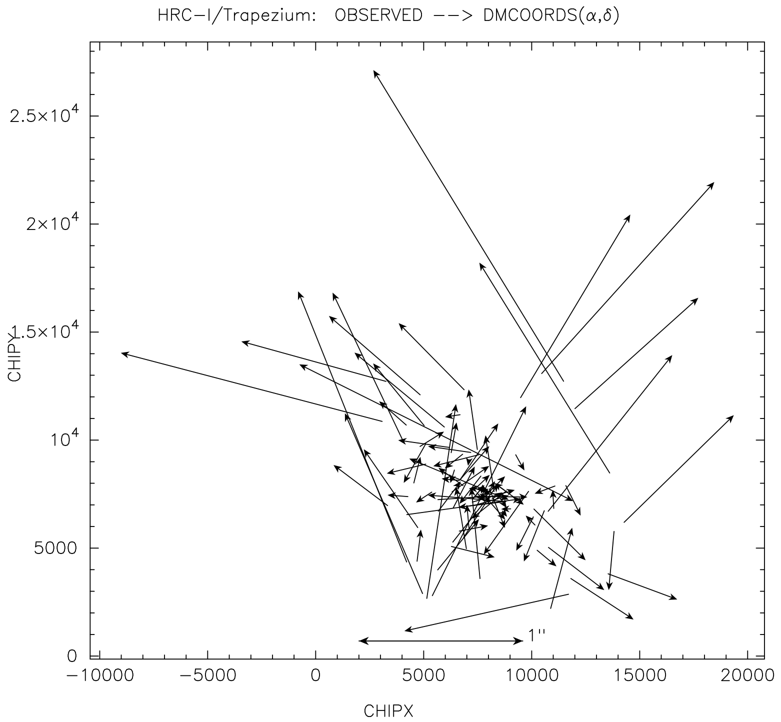

Figure 6. ONC: Positional shifts from observed centroids to the CHIP positions determined by *dmcoords* based on the optical astrometry and the nominal pointing of the telescope. The scaling convention follows that in Fig. 3.

We present here the *geomap* results, using the *rscale* functional form, which comprises a combination of a linear shift, a rotation, and a uniform magnification factor. In general, we find very good agreement between the 3 detector models, and a consistent difference between the *SAOsac* and *MARX* raytraces. Accordingly, we only include results for the *SAOsac/deticpt* and *MARX/MARX* configurations. Table 1 provides the *geomap* fits for the individual bright point source observations. Transformation parameters are given as the median of the 100 realizations; the errors we quote represent the range within which the central 70% of the realizations are found so they are similar to a Gaussian 1σ error. Treating the centroided CHIP positions of the sources as the reference coordinates, the transformations represent the required corrections to the simulations. We find an overall magnification of $\sim$0.03% for the *SAOsac* raytraces and $\sim$0.05% for *MARX*. The magnification, however, is dominated by the sources outside the central region of the plate. Fitting just the shifts of sources in the inner 5000x5000 pixel region yields a magnification of only $\sim$0.01% for *SAOsac* and $\sim$0.02% for *MARX*. Similarly, the lateral shifts of a few HRC pixels are dominated by larger shifts of the outside sources. A small rotation between the observations and simulations is seen, and is actually slightly larger for the inside sources.

Tables 2 and 3 show the transformation coefficients corresponding to the vector diagrams presented in Figures 4 and 5 for the ONC. The fits from the observed positions to simulated positions (Table 2) show a larger magnification effect for the inner region ($\sim$0.05% for *SAOsac*, $\sim$0.06 for *MARX*) than the outer region ($\sim$0.01% for *SAOsac*, $\sim$0.03% for *MARX*). The *geomap* transformations from the *dmcoords* positions to the simulated positions, shown in Table 3, yield results closer to those for the individual point sources. The magnification for the outside sources is about 0.04% for *SAOsac* raytraces and 0.06% for *MARX*. For the inner region of the HRC-I, there is a stretch of $\sim$0.02% for *SAOsac* and $\sim$0.03% for *MARX*. We also fit the offset between the observed centroids and the *dmcoords* positions based on the Hillenbrand 1997 catalog. Table 4 details those results, corresponding to the vector plot in Fig. 6. A magnification factor of -0.02% overall implies a correction to *dmcoords* that would serve to compress its output positions. *geomap* fits for the various ONC shifts seem to yield slightly higher values for a rotation, especially for the central region, at about 0.01° for both *SAOsac* and

MARX. Transformations between *dmcoords* positions and simulated positions yield lateral shifts and residual offsets after the *geomap* fits are performed that are comparable to those for the individual bright point sources. Lateral shifts and residual offsets are both larger for the fits between observed and simulated CHIP coordinates.

Table 1. Individual bright point sources: *geomap* results for 100 realizations, from observed centroids to simulated positions. This table corresponds to the vector diagrams of Fig. 3.

SAOsac + deticpt

region	Mag (%)	XSHIFT [pix]	YSHIFT [pix]	ROTATION [deg]	XRMS [pix]	YRMS [pix]
outside	$0.039\,^{+0.007}_{-0.006}$	$-2.684\,^{+0.785}_{-0.842}$	$-3.114\,^{+0.846}_{-0.785}$	$0.00017\,^{+0.00205}_{-0.00202}$	$0.876\,^{+0.182}_{-0.113}$	$0.910\,^{+0.140}_{-0.152}$
inside	$0.009\,^{+0.003}_{-0.002}$	$-1.100\,^{+0.232}_{-0.270}$	$-0.263\,^{+0.234}_{-0.215}$	$0.00398\,^{+0.00121}_{-0.00143}$	$0.213\,^{+0.022}_{-0.014}$	$0.202\,^{+0.013}_{-0.012}$
all	$0.033\,^{+0.005}_{-0.005}$	$-2.512\,^{+0.466}_{-0.386}$	$-2.563\,^{+0.580}_{-0.458}$	$0.00082\,^{+0.00185}_{-0.00151}$	$0.579\,^{+0.088}_{-0.079}$	$0.549\,^{+0.088}_{-0.082}$

MARX + MARX

region	Mag (%)	XSHIFT [pix]	YSHIFT [pix]	ROTATION [deg]	XRMS [pix]	YRMS [pix]
outside	$0.060\,^{+0.002}_{-0.003}$	$-5.277\,^{+0.394}_{-0.387}$	$-4.964\,^{+0.465}_{-0.339}$	$0.00206\,^{+0.00216}_{-0.00185}$	$0.606\,^{+0.097}_{-0.071}$	$0.616\,^{+0.092}_{-0.066}$
inside	$0.024\,^{+0.001}_{-0.001}$	$-3.073\,^{+0.133}_{-0.169}$	$-1.795\,^{+0.125}_{-0.146}$	$0.00538\,^{+0.00073}_{-0.00060}$	$0.202\,^{+0.008}_{-0.008}$	$0.187\,^{+0.005}_{-0.009}$
all	$0.052\,^{+0.002}_{-0.002}$	$-4.908\,^{+0.336}_{-0.170}$	$-4.324\,^{+0.317}_{-0.224}$	$0.00286\,^{+0.00163}_{-0.00174}$	$0.471\,^{+0.031}_{-0.047}$	$0.476\,^{+0.041}_{-0.028}$

Table 2. ONC: *geomap* results for 100 realizations, from observed centroids to simulated positions. This table corresponds to the vector diagrams of Fig. 4.

SAOsac + deticpt

region	Mag (%)	XSHIFT [pix]	YSHIFT [pix]	ROTATION [deg]	XRMS [pix]	YRMS [pix]
outside	$0.012\,^{+0.006}_{-0.006}$	$0.021\,^{+0.724}_{-0.710}$	$-3.695\,^{+0.488}_{-0.593}$	$0.00221\,^{+0.00200}_{-0.00244}$	$4.145\,^{+0.098}_{-0.098}$	$4.163\,^{+0.203}_{-0.133}$
inside	$0.047\,^{+0.004}_{-0.003}$	$-4.980\,^{+0.260}_{-0.272}$	$-2.245\,^{+0.293}_{-0.351}$	$0.01225\,^{+0.00101}_{-0.00127}$	$1.160\,^{+0.017}_{-0.020}$	$1.051\,^{+0.017}_{-0.015}$
all	$0.019\,^{+0.006}_{-0.005}$	$-1.603\,^{+0.622}_{-0.696}$	$-2.237\,^{+0.343}_{-0.485}$	$0.00558\,^{+0.00232}_{-0.00229}$	$2.988\,^{+0.062}_{-0.074}$	$3.262\,^{+0.130}_{-0.163}$

MARX + MARX

region	Mag (%)	XSHIFT [pix]	YSHIFT [pix]	ROTATION [deg]	XRMS [pix]	YRMS [pix]
outside	$0.029\,^{+0.002}_{-0.002}$	$-2.005\,^{+0.343}_{-0.360}$	$-5.438\,^{+0.262}_{-0.255}$	$0.00257\,^{+0.00112}_{-0.00113}$	$4.167\,^{+0.060}_{-0.046}$	$4.147\,^{+0.074}_{-0.070}$
inside	$0.061\,^{+0.001}_{-0.002}$	$-6.795\,^{+0.140}_{-0.109}$	$-3.834\,^{+0.174}_{-0.158}$	$0.01247\,^{+0.00080}_{-0.00070}$	$1.277\,^{+0.009}_{-0.009}$	$1.166\,^{+0.009}_{-0.012}$
all	$0.036\,^{+0.002}_{-0.002}$	$-3.616\,^{+0.279}_{-0.282}$	$-4.007\,^{+0.213}_{-0.214}$	$0.00604\,^{+0.00113}_{-0.00103}$	$3.020\,^{+0.044}_{-0.038}$	$3.253\,^{+0.054}_{-0.059}$

Table 3. ONC: *geomap* results for 100 realizations, from *dmcoords* positions to simulated positions. This table corresponds to the vector diagrams of Fig. 5.

SAOsac + deticpt

region	Mag (%)	XSHIFT [pix]	YSHIFT [pix]	ROTATION [deg]	XRMS [pix]	YRMS [pix]
outside	$0.040^{+0.006}_{-0.006}$	$-2.773^{+0.724}_{-0.711}$	$-3.020^{+0.488}_{-0.594}$	$0.00084^{+0.00200}_{-0.00243}$	$0.849^{+0.134}_{-0.117}$	$0.912^{+0.129}_{-0.097}$
inside	$0.019^{+0.004}_{-0.003}$	$-1.742^{+0.259}_{-0.272}$	$-0.970^{+0.293}_{-0.350}$	$0.00370^{+0.00101}_{-0.00127}$	$0.457^{+0.017}_{-0.011}$	$0.599^{+0.022}_{-0.014}$
all	$0.038^{+0.006}_{-0.005}$	$-2.704^{+0.621}_{-0.696}$	$-2.750^{+0.343}_{-0.486}$	$0.00104^{+0.00231}_{-0.00229}$	$0.694^{+0.088}_{-0.072}$	$0.795^{+0.080}_{-0.064}$

MARX + MARX

region	Mag (%)	XSHIFT [pix]	YSHIFT [pix]	ROTATION [deg]	XRMS [pix]	YRMS [pix]
outside	$0.056^{+0.002}_{-0.002}$	$-4.800^{+0.342}_{-0.360}$	$-4.764^{+0.262}_{-0.255}$	$0.00121^{+0.00112}_{-0.00113}$	$0.508^{+0.074}_{-0.065}$	$0.530^{+0.067}_{-0.064}$
inside	$0.033^{+0.001}_{-0.002}$	$-3.559^{+0.140}_{-0.109}$	$-2.560^{+0.174}_{-0.158}$	$0.00392^{+0.00080}_{-0.00070}$	$0.159^{+0.007}_{-0.008}$	$0.373^{+0.008}_{-0.009}$
all	$0.054^{+0.002}_{-0.002}$	$-4.718^{+0.279}_{-0.281}$	$-4.521^{+0.212}_{-0.214}$	$0.00149^{+0.00112}_{-0.00103}$	$0.417^{+0.055}_{-0.046}$	$0.480^{+0.044}_{-0.039}$

Table 4. ONC: *geomap* results for 100 bright sources, providing a transformation of *dmcoords* positions to map them to the observed centroids.

observed centroids –> *dmcoords* (α,δ)

Region	Mag (%)	XSHIFT [pix]	YSHIFT [pix]	ROTATION [deg]	XRMS [pix]	YRMS [pix]
outside	−0.028	2.793	−0.675	0.00136	4.219	4.141
inside	0.028	−3.234	−1.273	0.00855	1.316	1.196
all	−0.018	1.102	0.513	0.00454	3.070	3.251

5. SUMMARY AND CONCLUSIONS

5.1. Summary

Simulations of ∼160 observations of AR Lac, HR 1099, and LMC X-1 show that there is a magnification or platescale effect that is either unaccounted for by the CXC telescope models or an artifact of using *dmcoords* to determine off-axis and azimuthal angles for the simulations. A platescale error in the models could be explained by:

- Incorrect position of the detector in the simulations
- Incorrect effective focal length of the optics' models
- Incorrect HRC pixel size (6.4294 μm/pixel) in the *Chandra* Calibration Database[13](CALDB)
- Errors in the HRC degap map

A 0.03% magnification corresponds to a change in the focal length or an offset of the detector of roughly 3mm. Or it could correspond to a change in the HRC pixel size of ∼0.002 μm. A 0.05% change in platescale infers a 5mm change in focal length or a ∼0.003 μm change in pixel size. We can rule out an incorrect detector position in the simulations as the cause because changes of even 1mm would cause significant distortions of the

PSF, but studies of the on-axis PSF of AR Lac show excellent agreement with the models.[14] Distinguishing between the HRC pixel size and the mirror model's focal length would be made easier by carrying out these analyses on the ACIS detectors. It appears that there is a different platescale effect for the *MARX* and *SAOsac* raytraces, pointing to a difference between the two mirror models. It remains unclear what impact the drift of the ACA's fiducial lights might have on the ability of *dmcoords* or the various detector models to predict where a source will be imaged to the detector.

Looking at the Orion Nebular Cluster stars with well-determined relative positions provides more insight into how the *Chandra* mirrors image a grid of sources to the detector plane. When *dmcoords* is used to determine the CHIP coordinates for a source, based on the optical astrometry and pointing information, we see spatial transformations very similar to those for the bright point source observations and simulations. The positions of the simulations were determined from the optical star positions, and would presumably match the positions of the observations if the CXC mirror models and detector models were ideal. Figure 4 shows this is clearly not the case.

5.2. Conclusions and Further Study

The two different approaches to studying the optical distortions of *Chandra*'s mirrors yield fairly different results. Comparisons between observed detector locations and simulated positions, namely those in Fig. 3 and Fig. 4, show different types of magnification effects. For the individual bright point sources (Table 1), the magnification for the outside sources is $\sim$4 times greater than that for the inside sources. For the ONC, the reverse is true, and the magnification for the inside sources is $\sim$4 times greater than that for the outside sources (see Table 2). This could be an artifact of using *dmcoords* to determine off-axis and azimuthal angles for the simulations of the individual bright point sources. Since we simulate the ONC sources based on their optical astrometry, we have more confidence that the results for the ONC are a better measure of the optical distortions of *Chandra*'s mirrors. Similar results between the individual point sources and the ONC when we use *dmcoords* to predict a CHIP position further support this judgment.

We have not been able to isolate the optical distortions of the mirrors from other effects that we encounter. There are a variety of questions which we have not yet reconciled, including:

- the sensitivity to our centroiding technique versus a wavelet approach.
- the effect of the PSF shape on centroid position
- possible motion of the SIM with respect to the HRMA
- effects of the HRC degap map on CHIP positions themselves, with possible platescale effect
- our ability to independently and accurately assess the off-axis and azimuthal angle of a source
- reliance on a simple tangent plane correction between focal surface and detector
- uncertainty in position of the optical axis of the telescope

We intend to pursue these questions in order to establish a better diagnostic of *Chandra*'s optical distortions. We will look at cluster observations on other *Chandra* detectors to separate detector artifacts from the optics, adding some difficulty due to chip gaps and tilts associated with the HRC-S and ACIS. We will also study calibration observations including those used to determine the boresight, platescale, and optical axis, in order to ensure a consistent experiment.

ACKNOWLEDGMENTS

We are grateful to Ettore Flaccomio for making available his cross-correlations between the *Chandra* X-ray sources in the ONC and those from other catalogs.

This work was supported by NASA Contract NAS8-39073.

REFERENCES

1. L. A. Hillenbrand, "On the stellar population and star-forming history of the Orion Nebula Cluster," *Astron J.* **113**, pp. 1733-1768, 1997.
2. L. A. Hillenbrand and J. A. Carpenter, "Constraints on the stellar/substellar mass function in the inner Orion Nebular Cluster," *Astrophys J.* **540**, pp. 236-254, 2000.
3. *ChandraInteractive Analysis of Observations*, *Chandra* X-ray Center, `http://cxc.harvard.edu/ciao/`
4. J. McDowell, "Coordinate systems for analysis of on-orbit *Chandra* data", tech. rep., May 2001, `http://cxc.harvard.edu/contrib/jcm/ncoords.ps`
5. T. Aldcroft, "*Chandra* absolute astrometric accuracy", tech. rep., *Chandra* X-ray Center, June 2002, `http://cxc.harvard.edu/cal/ASPECT/celmon/`
6. E. Flaccomio, Università di Palermo, private communication, June 2003
7. T. Aldcroft, "Alignment drift during IRU swap and ACA cooldown", tech. rep., *Chandra* X-ray Center, Aug. 2003, `http://cxc.harvard.edu/mta/ASPECT/IRU_swap/fid_drift/`
8. D. Jerius, L. Cohen, R. J. Edgar, *et al.*, "The role of modeling in the calibration of *Chandra*'s optics", in *Proc. SPIE* **5165**, *X-Ray and Gamma-Ray Instrumentation for Astronomy XIII*, 2004. this volume.
9. M. W. Wise, J. E. Davis, D. P. Huenemoerder, J. C. Houck, and D. Dewey, "MARX 4.0 Technical Manual", Feb. 2003, `ftp://space.mit.edu/pub/CXC/MARX/v4.0/marx_4.0_manual.pdf`
10. "*psf_project_ray* Documentation", *Chandra* X-ray Center, `http://cxc.harvard.edu/ciao/ahelp/psf_project_ray.html`
11. "*deticpt* Documentation", CXC Optics Group, `http://hea-www.harvard.edu/MST/simul/software/docs/html/deticpt.html`
12. *Image Reduction and Analysis Facility*, National Optical Astronomy Observatories, `http://iraf.noao.edu/iraf-homepage.html`
13. *Chandra Calibration Database*, *Chandra* X-ray Center, `http://cxc.harvard.edu/caldb/`
14. D. Jerius, T. J. Gaetz, and M. Karovska, "Calibration of *Chandra*'s near on-axis performance", in *Proc. SPIE* **5165**, *X-Ray and Gamma-Ray Instrumentation for Astronomy XIII*, 2004. this volume.